NANO LETTERS

pubs.acs.org/NanoLett Letter

Enhanced Berry Curvature Dipole and Persistent Spin Texture in the Bi(110) Monolayer

Kyung-Hwan Jin,*[,‖] Eunseok Oh,[‖] Roland Stania,[‖] Feng Liu, and Han Woong Yeom*

Cite This: *Nano Lett.* 2021, 21, 9468−9475 Read Online

ACCESS | Metrics & More | Article Recommendations | Supporting Information

ABSTRACT: Nonvanishing Berry curvature dipole (BCD) and persistent spin texture (PST) are intriguing physical manifestations of electronic states in noncentrosymmetric 2D materials. The former induces a nonlinear Hall conductivity while the latter offers a coherent spin current. Based on density-functional-theory (DFT) calculations, we demonstrate the coexistence of both phenomena in a Bi(110) monolayer with a distorted phosphorene structure. Both effects are concurrently enhanced due to the strong spin−orbit coupling of Bi while the structural distortion creates internal in-plane ferroelectricity with inversion asymmetry. We further succeed in fabricating a Bi(110) monolayer in the desired phosphorene structure on the $NbSe_2$ substrate. Detailed atomic and electronic structures of the Bi(110)/$NbSe_2$ heterostructure are characterized by scanning tunneling microscopy/spectroscopy and angle-resolved-photoemission spectroscopy. These results are consistent with DFT calculations which indicate the large BCD and PST are retained. Our results suggest the Bi(110)/$NbSe_2$ heterostructure as a promising platform to exploit nonlinear Hall and coherent spin transport properties together.

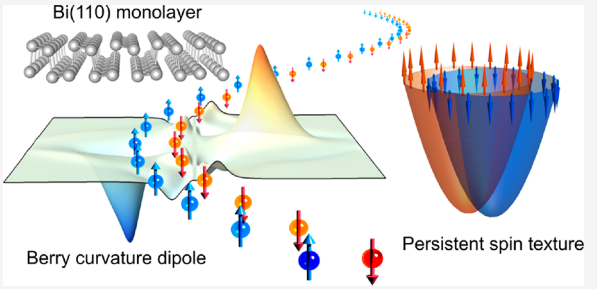

KEYWORDS: *Bi(110) monolayer, Berry curvature dipole, nonlinear Hall effect, persistent spin texture, heterostructure*

Rich and exotic electronic properties may arise through symmetry breaking in two-dimensional (2D) materials with strong interactions, which have recently attracted much attention for both fundamental interests and novel electronic/spintronic device concepts. For example, one intriguing physical manifestation of noncentrosymmetric 2D crystals, characterized with inversion symmetry breaking, is the nonzero Berry curvature dipole (BCD) despite an overall trivial topological state.[1] Under nonequilibrium electron distribution, the BCD leads to an intriguing nonlinear Hall signal, offering technological potential in nonlinear quantum devices with frequency doubling and rectification functions for energy harvesting, wireless communications, and Hall rectifier.[2−5] On the other hand, the inversion symmetry breaking induces a nonvanishing internal electric field in the bulk, which can combine with spin−orbit coupling (SOC) to generate a momentum-dependent magnetic field that acquires a persistent spin texture (PST). This spin structure offers electrical controllability over spins with long spin coherence.[6−8] So, BCD and PST render noncentrosymmetric 2D materials attractive for studying ferroelectricity,[9] nonlinear optical response,[10] and coherent spin transport.[11]

The BCD-induced nonlinear Hall effect has been proposed in several 2D materials, such as single layer transition metal dichalcogenides[12,13] and a SnTe monolayer,[14] and confirmed experimentally in a WTe_2 monolayer.[2,3] The PST has been reported in a few 1D defetcs[7,8] and 2D systems of group-IV monochalcogenides.[15,16] Although these two properties have been observed and discussed in different materials, they may be fundamentally related, since both require inversion asymmetry and strong SOC. Here, we show how these exotic properties are systematically connected and introduce a Bi(110) monolayer as an ideal material platform to host both phenomena. In order to make this proposal more practical beyond a freestanding form of 2D materials, possible effects of a substrate have to be considered. In particular, the interface with a substrate can introduce a vertical electric field (a conventional Rashba SOC effect) that is expected to interplay with the in-plane field to suppress or enhance both BCD and PST.

Using density functional theory (DFT) calculations, we predict the existence of in-plane ferroelectricity in a buckled Bi(110) monolayer due to the interplay between its low-symmetry structure and the strong SOC. The ferroelectricity induces a large BCD upon doping and, at the same time, an out-of-plane unidirectional PST. The DFT calculations also confirm that both BCD and PST are retained on a $NbSe_2$ substrate, which naturally dopes the overlayer to create BCD.

Received: July 20, 2021
Revised: November 3, 2021
Published: November 8, 2021

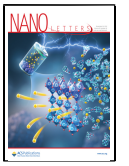

https://doi.org/10.1021/acs.nanolett.1c02811
Nano Lett. 2021, 21, 9468−9475

Furthermore, we demonstrate the successful epitaxial growth of the Bi(110) monolayer with the desired phosphorene structure on a $NbSe_2$ substrate by molecular beam epitaxy (MBE). The structural and electronic properties of the Bi(110)/$NbSe_2$ heterostructure are characterized by scanning tunneling microscopy/spectroscopy (STM/STS) and angle-resolved photoemission spectroscopy (ARPES), which identified the heterostructure's structural model and the salient band features, respectively, consistent with DFT calculations.

RESULTS AND DISCUSSION

Atomic and Electronic Structure of the Bi(110) Monolayer. The Bi(110) monolayer crystallizes with a distorted phosphorene structure that belongs to the nonsymmorphic space group $Pmn2_1$,[17−20] containing several symmetry operations of glide planes and screw axes (see Table 1). The optimized lattice constants are a = 4.90 Å and b = 4.59 Å, which agree well with the experimental[21−23] and theoretical[17,18,20] results reported. A notable structural feature is the finite out-of-plane buckling (Figure 1a), resulting from the vertical shift of the two centered Bi atoms. This buckling, as confirmed by DFT calculation and experiment, is the key factor in determining its topological properties[21,22,24,25] and is sensitive to electron/hole doping (Figure S1). Figure 1b,c shows the calculated band structures of the flat and puckered Bi(110) structure, respectively. They are both semiconductors with band gaps of 0.09 and 0.25 eV, respectively. In the flat structure, all bands are doubly degenerated protected by inversion symmetry, whereas in the buckled structure, the band degeneracy is lifted by inversion symmetry breaking except for the Γ−X direction in the Brillouin zone (BZ). One can understand the lifted degeneracy from the group symmetry of $\bar{M}_{010}$ and $\tilde{\Theta} \equiv T\bar{M}_{010}$; $\tilde{\Theta}^2 \equiv T^2\bar{M}_{010}^2 = 1$ along the Γ−Y [$\mathbf{k}$= (0, k_y)] to make the Bloch states $\Psi_{\mathbf{k}}$ and $\Theta\Psi_{\mathbf{k}}$ nondegenerate. Subsequently, each state can be labeled using the eigenvalues of $\bar{M}_{100}$; $M_{100}|\Psi_{\mathbf{k}}^{\pm}\rangle = \pm ie^{-ik_y/2}|\Psi_{\mathbf{k}}^{\pm}\rangle$ since $\bar{M}_{100}^2 = -e^{-ik_y}$. Therefore, there are four nondegenerate Bloch states along the Γ−Y line, which can be clearly seen near the Y point. In contrast, the bands along the Γ−X line remain doubly degenerate because they are protected by T and $\bar{M}_{100} = \left\{M_{100}\middle|0, \frac{1}{2}, \frac{1}{2}\right\}$ mirror symmetry. Namely, along the line $\mathbf{k}$ = (k_x, 0), k_x is invariant under the transformations of M_{010} and $\Theta \equiv T\bar{M}_{100}$. Since $T^2 = -1$ for a spin-half system and $\Theta^2 \equiv T^2\bar{M}_{100}^2 = e^{-ik_y} = -1$, all bands are doubly degenerate along Γ−X. The doublet states ($\Psi_{\mathbf{k}}$, $\Theta\Psi_{\mathbf{k}}$) form a Kramers pair. The anisotropic band splitting is clearly shown in Figure 1d and Figure S2.

We further investigate the effect of an out-of-plane external electric field E_z on the band structure since the Bi(110) monolayer, for most of the experimental characterization and device fabrication, has to be grown on or transferred onto a suitable substrate, which would inevitably introduce an *external* out-of-plane electric field at the interface. The interfacial electric field is important in the present case since it can induce a conventional Rashba effect to interplay or interfere with a new form of Rashba effect induced by the *internal* in-plane electric field, which will be discussed below. Figure 1e−g

Table 1. Symmetries of Puckered Bi(110) Structure with Nonsymmorphic Space Group $Pmn2_1$ (No. 31)

symmetry	(x, y, z) form	operation
identity	(x, y, z)	{1|0}
mirror	x, $-y$, z	$\{M_{010}\|0\} \equiv M_{010}$
glide plane	$-x$, y + 1/2, z + 1/2	$\{M_{100}\|0, 1/2, 1/2\}$
rotation	$-x$, $-y$ + 1/2, z + 1/2	$\{2_{001}\|0, 1/2, 1/2\}$

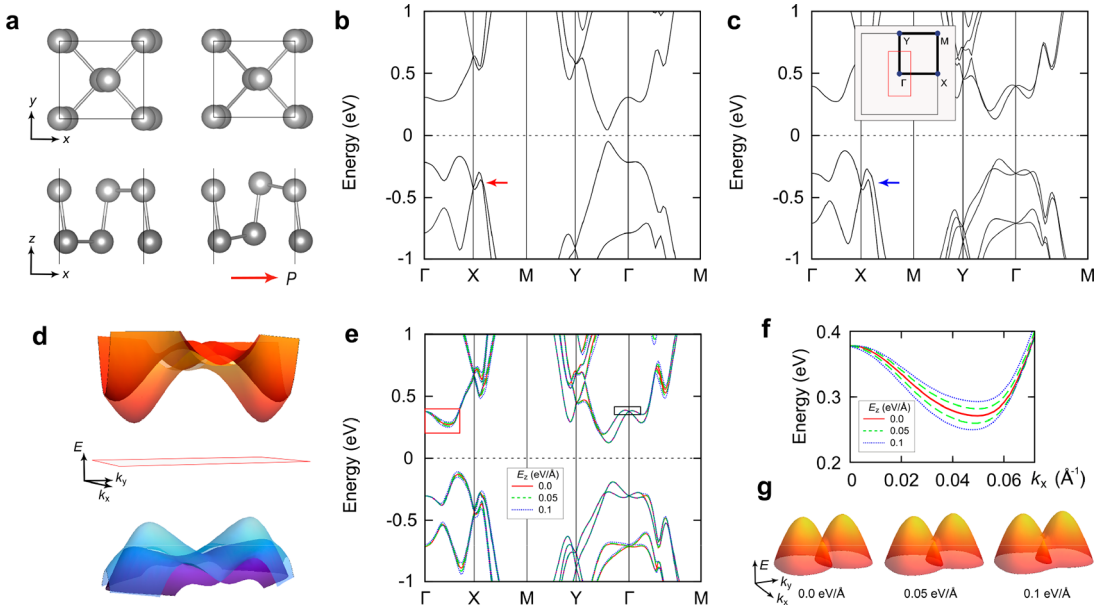

Figure 1. Atomic structure and electronic structure of the Bi(110) monolayer. (a) Top and side views of atomic structures of flat and puckered Bi(110) monolayer. (b, c) Calculated band structure of flat and puckered Bi(110) monolayer, respectively. The inset in *c* shows the BZ. The red (blue) arrow indicates the crossing point (SOC gap) along the X−M path. (d) 3D band plot of the puckered Bi(110) near the Γ point as indicated by the red line in the inset of (c). (e) Calculated band structure of the puckered Bi(110) monolayer under different out-of-plane electric fields, E_z = 0.0, 0.05, and 0.1 eV/Å. (f) Enlarged band structure as indicated by the red box in (e). (g) 3D band plot near the Γ point as indicated by the black box in (e).

https://doi.org/10.1021/acs.nanolett.1c02811
Nano Lett. 2021, 21, 9468−9475

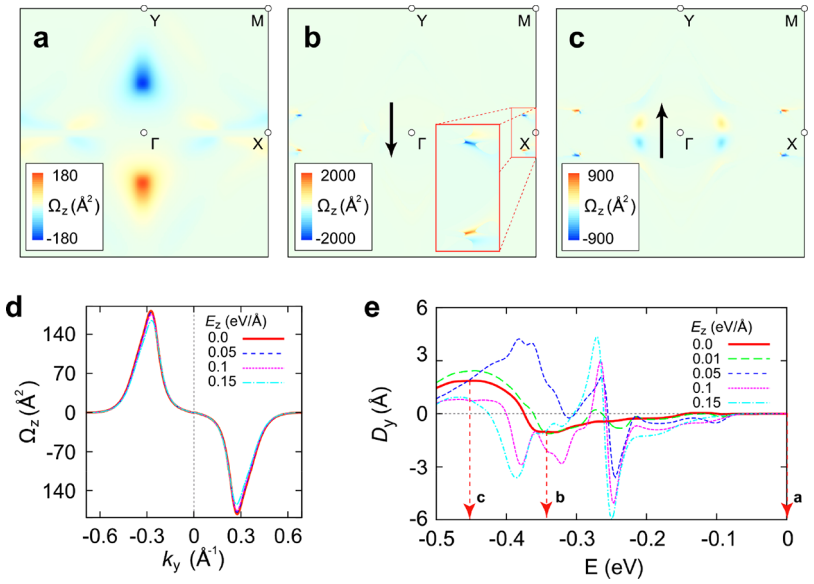

Figure 2. Berry curvature properties of the Bi(110) monolayer. The calculated Berry curvature $\Omega_z(\mathbf{k})$ of the puckered Bi(110) monolayer in the first Brillouin zone (BZ) at different Fermi energies; (a) $E = 0$ eV (all valence bands occupied), (b) $E = -0.34$ eV, and (c) $E = -0.45$ eV (parts of the valence bands are empty). The black arrow shows the direction of BCD vector D_y. (d) BC that is calculated along the −Y−G−Y line in under varying the out-of-plane electric fields (E_z). (e) Calculated BCD (D_y) of the puckered Bi(110) monolayer with varying E_z. The Fermi level (E = 0 eV) is based on the middle of the band gap of the Bi(110) monolayer.

shows the evolution of band structures of the puckered Bi(110) monolayer under an out-of-plane electric field. There are no significant changes except for the bands along the Γ−X line. The band degeneracy along the k_x direction is lifted because the glide mirror symmetry $\bar{M}_{100}$ is now broken.

BCD and Nonlinear Anomalous Hall Effect. Next, we analyze the band topology in terms of the Berry curvature. In general, a system is topologically trivial when the Berry curvature of all occupied bands is summed to zero. In a 2D system with time-reversal symmetry preserved but inversion symmetry broken, one interesting case occurs when the Berry curvature distribution in BZ is featured with two local peaks of opposite signs. Upon hole doping, they give rise to a nonzero BCD, even though the total sum of BC is zero.[14] The BCD in 2D can be expressed as[1]

$$D_a = \int \mathrm{d}\mathbf{k}\, f(\mathbf{k}) \frac{\partial \Omega_z(\mathbf{k})}{\partial \mathrm{k}_a} \tag{1}$$

where $f(\mathbf{k})$ is the Fermi Dirac distribution, $\Omega_z(\mathbf{k})$ is the z component of BC, and $a = x, y$. We have calculated the Berry curvature distribution $\mathbf{\Omega}(\mathbf{k}) = \Omega_z\hat{z}$ and the resulting BCD in the puckered Bi(110) monolayer, as shown in Figure 2. Figure 2a displays the distribution of Berry curvature Ω_z of all occupied bands in the BZ, by setting the Fermi level at zero energy. Interestingly, a pair of positive and negative peaks appears along the Γ−Y line, indicating the existence of a finite BCD. They are composed of the y-component (D_y) only, which is perpendicular to the mirror plane since $\partial\Omega_z/\partial k_x$ is odd to M_{010} while $\partial\Omega_z/\partial k_y$ is even with $\Omega_z(\mathbf{k})$ given to be odd with respect to the M_{010} (see Supporting Information Figure S3). Such bipolar configuration of the Berry curvature is subjected to the M_{010} symmetry and, thus, is not affected significantly by the increase of the out-of-plane electric field E_z (Figure 2d). On the other hand, the direction of Berry curvature polarization reverses when the structural distortion is reversed (see Supporting Information Figure S4). This indicates that the BCD is directly coupled with the ferroelectricity induced by the structural distortion that determines the direction of the internal in-plane electric field.

We show the corresponding BCD as a function of different energy levels in Figure 2e. Without doping, i.e., the Fermi level lies in the gap, the total BCD is always zero. With doping, i.e., the Fermi level lies below the top of the valence band, a finite BCD emerges. The Berry curvature distribution at each Fermi level position is shown in Figure 2b,c, respectively. Especially, in the absence of out-of-plane electric field ($E_z = 0$), there is one negative (positive) amplitude at $E = -0.34$ eV (-0.45 eV). The negative one at $E = -0.34$ eV is revealed to be predominantly contributed by the small-gap region near the X point (Figure 2b), which is related to the band crossing point along the X−M direction without SOC (Figure 1b and Figure S5). The SOC is crucial to enhance BCD by opening a gap at such a crossing point. The calculated BCD value is $D_y \sim 1$ Å, which is larger than the previously reported values of T_d-WTe_2 (0.1−3 Å)[12,26] and SnTe (0.3 Å).[14] At $E = -0.45$ eV, the pair of positive and negative Berry curvature peaks is reversed and the BCD changes sign. We further plot the Ω_z under different out-of-plane electric fields in Figure 2d for comparison. One notes that Ω_z of occupied bands does not change significantly with the increasing field. On the other hand, Ω_z and BCD depend strongly on the position of the Fermi level (namely, the doping level) and the out-of-plane electric fields (E_z), as shown in Figure 2e. As E_z increases, the BCD varies monotonically for -0.23 eV $< E < 0$ but nonmonotonically in other energy ranges. Interestingly, the magnitude of BCD is greatly enhanced at $0 \sim -0.3$ eV. Positioning the Fermi level in the corresponding energy range (hole doping) can be achievable with a $NbSe_2$ substrate, which will discussed later. The monotonic increase is caused by the emergence of additional nonzero BCD under the out-of-plane electric field. Under the applied field, the glide mirror plane symmetry $\bar{M}_{100}$ is broken to lift the band degeneracy along the X−M, which is protected by this symmetry. As a result, near $E \sim -0.23$ eV,

https://doi.org/10.1021/acs.nanolett.1c02811
Nano Lett. 2021, 21, 9468−9475

extra band touching points appear along the X−M line, contributing to a stronger BCD (see Supporting Information Figure S5).

An important consequence of nonzero BCD is the nonlinear anomalous Hall effect. Specifically, the nonlinear Hall current is proportional to the BCD moment at the Fermi surface. Therefore, the bipolar BC distribution in the puckered Bi(110) monolayer is expected to induce a nonlinear Hall current along the Bi zigzag chain direction (the y direction, along which the BCD is formed) in response to an oscillating electric field. For the realization of a strong nonlinear Hall signal in the Bi(110) bilayer, a promising approach is to grow a Bi(110) bilayer on a substrate to form a heterostructure, which induces an out-of-plane interfacial electric field and hole doping at the same time.

PST in the Ferroelectric Bi(110) Monolayer. As mentioned above, the anisotropic band splittings are associated with a spontaneous in-plane polarization P_s of the puckered structure upon inversion symmetry breaking. The polarization field is constrained within the x-direction defined by the mirror or glide mirror symmetries. The calculated P_s is 0.47×10^{-10} C/m, which is quite sizable.[27] More interestingly, the in-plane ferroelectricity induces a momentum-independent spin orientation known as PST.[6,15,28] As shown in Figure 3a, a unidirectional Rashba-type spin splitting is observed along the k_y-direction near the Γ point. Given the expectation value of spin operators $\langle S_a(\mathbf{k})\rangle = \left(\frac{\hbar}{2}\right)\langle\Psi_\mathbf{k}|\sigma_a|\Psi_\mathbf{k}\rangle$ $(a = x, y, z)$, the glide mirror symmetry $\bar{M}_{100}$ allows the z spin component only in each spin-polarized band. By carefully examining the spin textures calculated at a constant-energy cut-off $E = 0.37$ eV, we reveal that the z spin polarization persists not just along the specific k-path but over the entire BZ (Figure 3b and Figure S2).

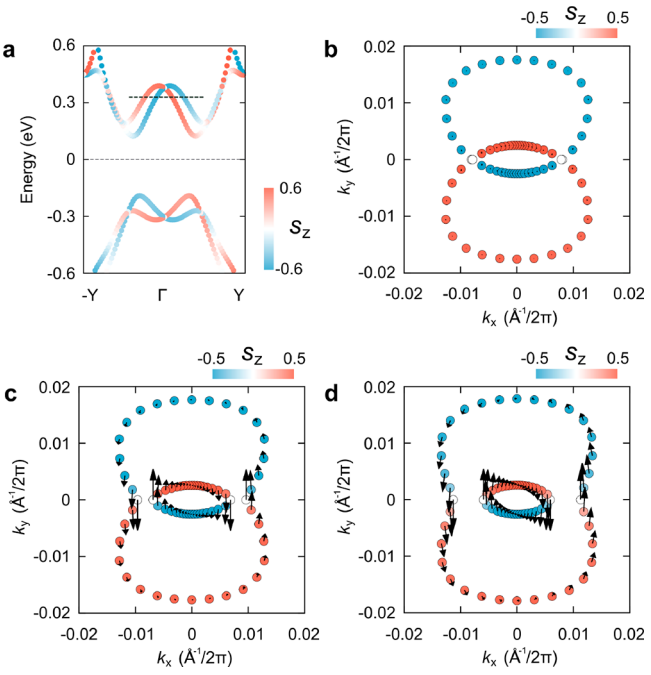

Figure 3. Spin texture of the Bi(110) monolayer. (a) Spin resolved band structure of the puckered Bi(110) monolayer along the Γ−Y direction. (b) Spin texture measured at the constant-energy cut-off $E = 0.37$ eV as indicated by dashed line in (a). The in-plane polarization induces the unidirectional (z-direction) spin polarized spin texture. (c, d) Spin texture measured for the out-of-plane electric field $E_z = 0.05$ eV/Å and $E_z = 0.1$ eV/Å at the constant-energy cut-off $E = 0.37$ eV, respectively.

The PST in elemental Bi(110) found here is quite unique, since the ferroelectricity and unidirectional spin configuration have usually been observed in compound 2D materials, such as SnSe and SnTe.[15,16,29] In general, the unidirectional spin texture can be understood by an effective model with the SOC Hamiltonian $H_{SOC} = (\alpha/\hbar)(\mathbf{E}\times\mathbf{p})\cdot\boldsymbol{\sigma}$ and $\mathbf{E} = \nabla V$, where α is a system-dependent SOC strength, $\mathbf{E}$ is an effective field, $\mathbf{p}$ is the momentum, and $\boldsymbol{\sigma}$ is the Pauli matrices. Depending on the field direction, a variety of SOC Hamiltonians are possible.[7,8,15,16] The conventional Rashba SOC effect has an out-of-plane electric field $\mathbf{E} = E_z\hat{z}$, leading to an in-plane helical spin texture. However, the polarization in the puckered Bi(110) monolayer is in-plane to produce an in-plane electric field $\mathbf{E} = E_x\hat{x}$. Thus, the effective model Hamiltonian can be written as $H = H_0 + H_{SOC} = \frac{\hbar^2}{2m}(k_x^2 + k_y^2) + (\alpha/\hbar)E_x k_y \sigma_z$. The in-plane field induces a form of the Rashba effect with z spin polarization as it separates the two parabolic bands. This leads to the unidirectional out-of-plane PST (see Supporting Information Figure S6). This spin texture suppresses the Dyakonov−Perel mechanism of spin relaxation, potentially ensuring a long-lived spin mode.[6] In line with the above discussion of the heterostructure, we further investigated the effect of an out-of-plane external electric field E_z on the PST. While the spin texture develops a more complex pattern, as shown in Figure 3c,d, the z spin polarization remains dominant with some in-plane helical spin components in the vicinity of the k_x axis.

Bi(110) Films Grown on the $NbSe_2$ Substrate. In spite of its interesting electronic properties, the experimental realization of a freestanding and doped Bi(110) puckered monolayer is expected to be challenging. Alternatively, we suggest a puckered Bi(110) film can be grown on a substrate with both large BCD and out-of-plane PST maintained. Figure 4b presents a topographic STM image of 1−3 layer (L) Bi films on $NbSe_2$. The step height of the Bi 1L film is measured to be ∼7.4 Å, compatible with the Bi(110) monolayer formation. Under the given growth condition, the 3L films are rarely formed, while the areal occupations of 1 and 2L are about 52 and 32%, respectively. From other large-scale topography, it is further confirmed that the portion of the 1L area is dominant (Figure S7). Parts (c, e) and (d, f) of Figure 4 show the high-resolution empty- and filled-state STM images of the Bi(110) 1L film, respectively. In the empty state, stripe patterns with different contrasts appear, which indicate unambiguously a Bi(110) film in clear contrast to the hexagonal structure expected for a Bi(111) film. The filled-state images display very different topographies, which will be explained below. The atomic resolution STM image indicates that the zigzag Bi chains run along the zigzag direction of a $NbSe_2$ substrate (y direction). In addition, a Moiré pattern is noticed with a period of ∼16 Å in both biases (the contrast modulation of strips in Figure 4e and that of bright clusters in Figure 4f), which would naturally originate from the lattice matching of a Bi(110) layer and the triangular $NbSe_2$ substrate. The Moiré pattern observed corresponds to a heterostructure between a 6×3 Bi(110) monolayer and a $5\sqrt{3} \times 4$ $NbSe_2$ substrate surface. Figure 4a shows the DFT-optimized structure of such a heterostructure, consistent with X-ray photoelectron diffraction results (Figure S8). The two Bi

https://doi.org/10.1021/acs.nanolett.1c02811
Nano Lett. 2021, 21, 9468−9475

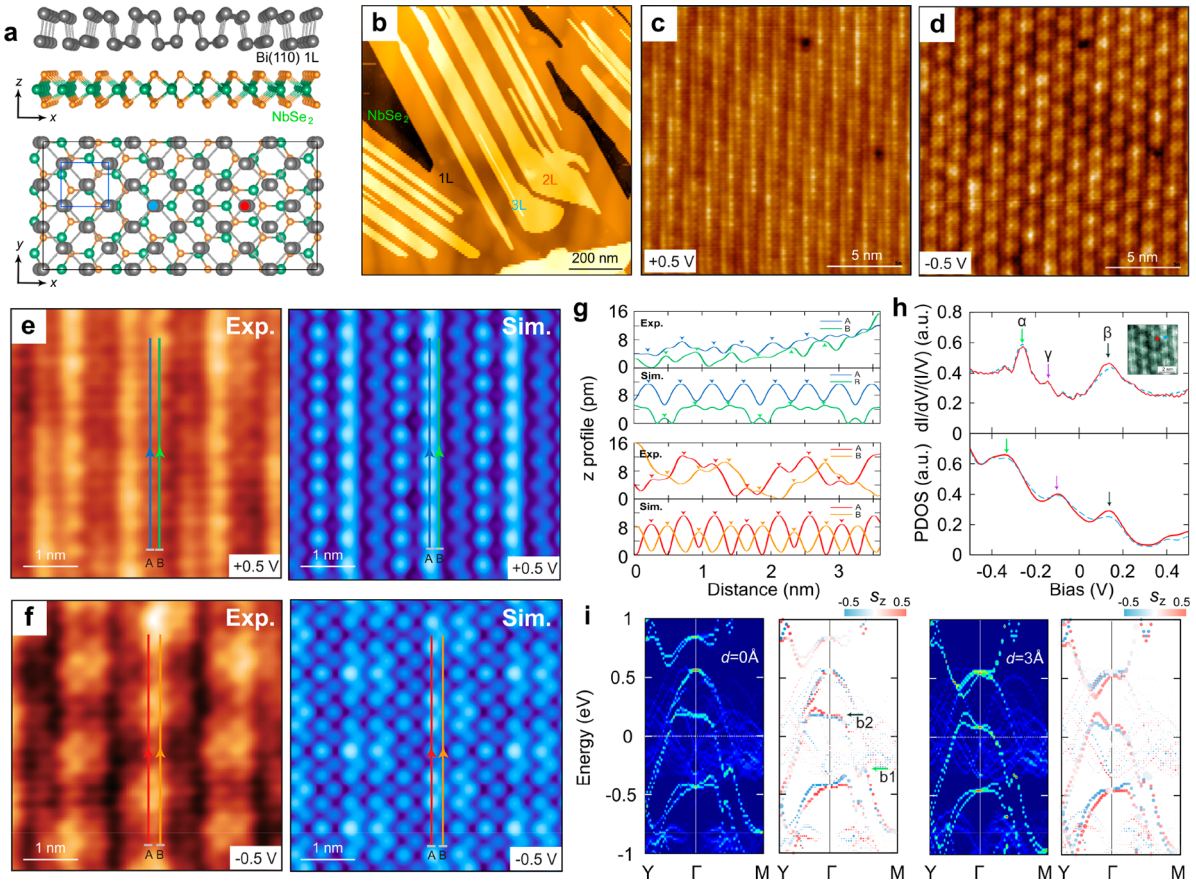

Figure 4. Bi/$NbSe_2$ heterostructure model and the corresponding STM images. (a) Side and top views of the Bi/$NbSe_2$ structural model consisting of a 6×3 Bi(110) monolayer on a $5\sqrt{3} \times 4$ $NbSe_2$ substrate. (b) STM morphology of Bi(110) films grown on a $NbSe_2$ substrate (constant-current mode with V_{bias} = +0.5 V, I_t = 100 pA, and 4.3 K). A narrow-area STM image of the Bi(110) 1L surface at (c) V_{bias}= +0.5 V, I_t = 5000 pA, and 4.43 K and (d) V_{bias}= −0.5 V, I_t = 5000 pA, and 4.43 K, respectively. (e) Atomically resolved STM image of the Bi(110) monolayer surface (left panel) for V_{bias} = +0.5 V and simulated STM image by integrating the orbitals from the Fermi level to 0.5 eV (right panel). (f) Atomically resolved STM image of the Bi(110) surface (left panel) for V_{bias} = −0.5 V and simulated STM image by integrating the orbitals from the Fermi level to −0.5 eV (right panel). (g) Experimental and simulated line profiles taken along the arrow marked in (e) and (f). (h) $dI/dV/(I/V)$ spectra at fixed positions and projected DOS (PDOS) of the Bi atoms indicated by blue and red points in (a). The normalized dI/dV curves are taken from the bright and dark areas of the Moiré pattern as indicated by the blue and red points in the inset image, respectively. (i) Unfolded band structure and the corresponding spin-resolved band structure of the heterostructure Bi/$NbSe_2$ model into the Brillouin zone of the Bi(110) monolayer unit cell for the equilibrium (d = 0 Å) and increased (d = 3 Å) bonding distance, respectively.

atoms in each sublayer are buckled, similar to a freestanding Bi(110) monolayer. This heterostructure model can be confirmed by the detailed comparison of experimental and calculated data; the simulated STM images for the empty and filled state match well the topographies measured (Figure 4e,f). Furthermore, the calculated charge corrugation agrees reasonably well with the STM line profile measured (Figure 4g), especially for the period of peaks (~4.6 Å) and their modulations.

In order to reveal further the electronic structure of the Bi film, we measure the STS [$dI/dV/(I/V)$] data on two different areas of monolayer Bi(110)/$NbSe_2$ (Figure 4h). Normalized dI/dV curves indicate major spectral features at about −0.25 eV (α), −0.18 eV (γ), and 0.18 eV (β), respectively, with the metallic tunneling property. These three states are well reproduced in the partial density of states (PDOS) projected onto the Bi(110) layer in the DFT calculations for the present heterostructure model (the bottom panel of Figure 4h). The origins of these spectral features can be found in the band structure of Bi(110)/$NbSe_2$. We unfolded the complicated band dispersions of the large Bi(110)/$NbSe_2$ supercell on the primitive cell of Bi(110), as shown in Figure 4i and Figure S9, for the equilibrium interfacial distance (d = 0 Å) and an artificially increased interfacial distance (d = 3 Å). At a large interfacial distance, which minimizes the interfacial hybridization of the bands, the band structure is a simple superposition of the bands from a bare Bi(110) monolayer and a $NbSe_2$ substrate. Comparing this band structure with that of the equilibrium distance, one can notice the upward shift of the band by the interfacial charge transfer due to the work function difference of Bi(110) and $NbSe_2$ (Figure S9 and Figure S10). The electrons are transferred from Bi(110) to the substrate that induces a hole type of Bi(110) band structure. In addition, at equilibrium distance, the interfacial coupling slightly reshapes the bands with splitting around 0.5 eV, but other valence and conduction states are maintained (Figure S9). We note that α and β peaks come mainly from the valence bands of a pristine Bi(110) monolayer (b1 and b2 in Figure 4i). The experiment further indicates that the Moiré superstructure modulates mainly the β peaks (Figure 4h), the top of the pristine valence band, which is also reproduced in the calculation.

https://doi.org/10.1021/acs.nanolett.1c02811
Nano Lett. 2021, 21, 9468−9475

We further measure the electronic band dispersions directly by ARPES. Figure 5a,b presents the photoemission intensities

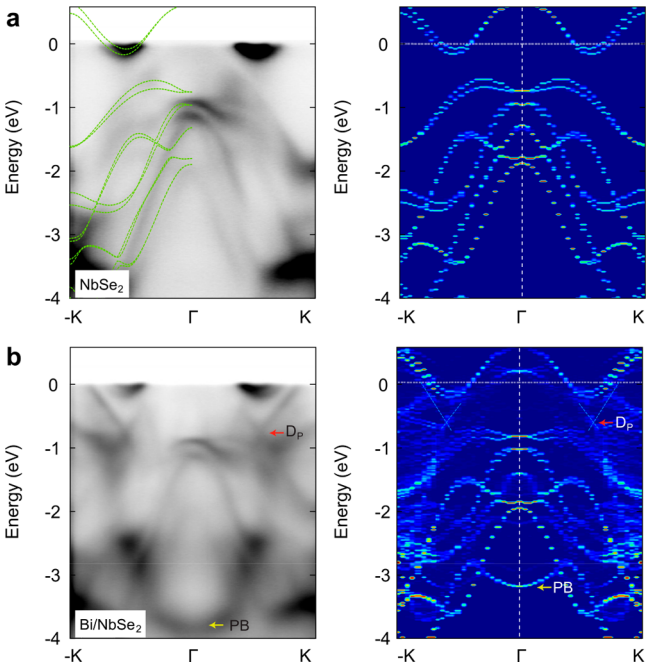

Figure 5. Reshaped band structure of the $Bi/NbSe_2$ heterostructure. (a) Photoemission intensity and calculated band structure for pristine $NbSe_2$, respectively. Green dashed lines overlaid on top of the ARPES map are the calculated band dispersions. (b) Photoemission intensity and unfolded band structure into primitive $NbSe_2$ BZ for heterostructure $Bi(110)/NbSe_2$, respectively.

of a pristine $NbSe_2$ substrate and the $Bi(110)/NbSe_2$ heterostructure along the Γ−K cut in the BZ, respectively. Since Bi(110) films are grown as islands on $NbSe_2$, one has to consider the bands from both contributions for experiments on the $Bi(110)/NbSe_2$ heterostructure. Our ARPES band dispersions for the pristine $NbSe_2$ substrate are fully consistent with the previous reports,[30,31] with electron pockets and the energy gap below them. The ARPES results are qualitatively reproduced by our DFT calculations as added in the figure. After deposition of the Bi(110) film, one can clearly observe the extra bands, most notably, a Dirac band (D_p) and a parabolic band around −0.8 eV and −3.8 eV, respectively (Figure 5b). The Dirac band is originated from the Bi 6*p* orbitals and well captured by the unfolded band structure of the calculation for the heterostructure (left panel of Figure 5b). The origin of the linear dispersion originates from the band dispersion of the Bi(110) monolayer located at $E \sim -0.7$ eV near the Y point (left panel of Figure 4i and Figure S11). We note that the calculated energy of the parabolic band at Γ deviates from the experimental result, which is likely due to the well-known limitation of GGA functionals in reproducing the band gap. It should also be noted that the unfolding is done on the unit cell of $NbSe_2$, which means that the unfolded band structure does not exactly correspond to that of the Bi(110) primitive cell; in the ARPES measurements, the BZ of $NbSe_2$ is more accurately determined by the Fermi surfaces of its electron pockets.

The overall agreement between the STS and ARPES experiments and the DFT calculation based on the present heterostructure model is excellent and provides strong support of the model and the electronic structure predicted. Although there are no direct experimental measurements of BCD and PST in the present study, the DFT calculations show that the BCD is retained in the $Bi(110)/NbSe_2$ heterosystem with $D_y \sim 2$ Å (see Supporting Information Figure S12). The calculated spin texture of the Bi(110) monolayer also maintains unidirectional (*z*-polarized) property even in the presence of the $NbSe_2$ substrate (Figure 4i). These experimental and theoretical results strongly indicate that the $Bi(110)/NbSe_2$ heterostructure is a unique material realization of BCD and PST together. It is expected that circular dichroism and spin-resolved ARPES experiments can directly confirm BCD and PST in the Bi(110) monolayer when its Fermi level is properly tuned. It was recently proposed that the energy band crossing (tilted Weyl points) near the Fermi level is crucial to generate a nonvanishing BCD,[13,32] and an external electric field can enhance the BCD by the band structure tuning.[26] In the $Bi(110)/NbSe_2$ heterostructure, an external electric field is applied by the $NbSe_2$ substrate and in the meantime band crossing points are induced by interlayer hybridization, leading to enhanced BCD with retained PST. Generally speaking, the van der Waals heterostructures with proper material combinations can offer a very practical and efficient route for the BCD engineering and efficient spin manipulation in a 2D system. That is, vertical stacking of 2D materials may allow for sensitive band structure engineering by tuning the interlayer hybridization and induce unique electronic and topological properties.[33−38]

CONCLUSIONS

In summary, based on first-principles calculations, the coexistence of enhanced BCD and PST is discovered in a buckled Bi(110) monolayer, in association with intriguing in-plane ferroelectricity. Our theoretical analysis reveals the underlying mechanism based on the interplay between the breaking of inversion symmetry and the strong SOC in Bi(110). We further show that such novel electronic properties can be secured in a Bi(110) film grown on a proper substrate such as a $Bi(110)/NbSe_2$ heterostructure. We indeed fabricate a $Bi(110)/NbSe_2$ heterostructure with a desired structure via molecular beam epitaxy, which is fully characterized by STM/STS and ARPES measurements. The detailed atomic structure of the $Bi(110)/NbSe_2$ heterostructure in STM and its electronic structure in STS and ARPES data are well reproduced by first-principles calculations based on our heterostructure model. The $Bi(110)/NbSe_2$ heterostructure provides a promising platform for realizing a sizable BCD and nonlinear Hall effect. Additionally, given the superconducting nature of $NbSe_2$, the $Bi(110)/NbSe_2$ heterostructure could be an interesting system for future investigation of topological superconductivity and exotic Majorana Fermionic excitations.

ASSOCIATED CONTENT

Supporting Information

The Supporting Information is available free of charge at https://pubs.acs.org/doi/10.1021/acs.nanolett.1c02811.

Computational and experimental methods, electron/hole doping dependent stability, the SOC splitting of the valence and conduction bands, the distribution of the Berry curvature gradient, Berry curvature with the opposite polarization, band structures of the Bi(110) monolayer under an out-of-plane electric field, the

https://doi.org/10.1021/acs.nanolett.1c02811
Nano Lett. 2021, 21, 9468−9475

conventional Rashba and out-of-plane Rashba model, large-scale topography, surface characterization via XPD, interface effect on band structures, charge density difference of the Bi/$NbSe_2$ interface, origin of the linear dispersion, and the BCD for Bi/$NbSe_2$ heterosystem (PDF)

AUTHOR INFORMATION

Corresponding Authors

Kyung-Hwan Jin − *Center for Artificial Low Dimensional Electronic Systems, Institute for Basic Science (IBS), Pohang 37673, Republic of Korea;* orcid.org/0000-0002-5116-9987; Email: khwanjin@gmail.com

Han Woong Yeom − *Center for Artificial Low Dimensional Electronic Systems, Institute for Basic Science (IBS), Pohang 37673, Republic of Korea; Department of Physics, Pohang University of Science and Technology, Pohang 37673, Republic of Korea;* orcid.org/0000-0002-8538-8993; Email: yeom@postech.ac.kr

Authors

Eunseok Oh − *Center for Artificial Low Dimensional Electronic Systems, Institute for Basic Science (IBS), Pohang 37673, Republic of Korea; Department of Physics, Pohang University of Science and Technology, Pohang 37673, Republic of Korea*

Roland Stania − *Center for Artificial Low Dimensional Electronic Systems, Institute for Basic Science (IBS), Pohang 37673, Republic of Korea*

Feng Liu − *Department of Materials Science and Engineering, University of Utah, Salt Lake City, Utah 84112, United States;* orcid.org/0000-0002-3701-8058

Complete contact information is available at: https://pubs.acs.org/10.1021/acs.nanolett.1c02811

Author Contributions

K.-H.J. and H.W.Y. conceived the research idea and plan. K.-H.J. performed the first-principles and model calculations. E.O. performed the STM experiment. R.S. performed ARPES experiments. All authors contributed to the interpretation and the discussion of the results. K.-H.J., F.L., and H.W.Y. prepared the manuscript with comments from all other authors.

Author Contributions

‖K.-H.J., E.O., and R.S. contributed equally.

Notes

The authors declare no competing financial interest.

ACKNOWLEDGMENTS

This work was supported by the Institute for Basic Science (Grant No. IBS-R014-D1). K.-H.J. is supported by the Institute for Basic Science (Grant No. IBS-R014-Y1). F.L. acknowledges the support from US-DOE (Grant No. DE-FG02-04ER46148).

REFERENCES

(1) Sodemann, I.; Fu, L. Quantum Nonlinear Hall Effect Induced by Berry Curvature Dipole in Time-Reversal Invariant Materials. *Phys. Rev. Lett.* **2015**, *115* (21), 216806.

(2) Xu, S.-Y.; Ma, Q.; Shen, H.; Fatemi, V.; Wu, S.; Chang, T.-R.; Chang, G.; Valdivia, A. M. M.; Chan, C.-K.; Gibson, Q. D.; Zhou, J.; Liu, Z.; Watanabe, K.; Taniguchi, T.; Lin, H.; Cava, R. J.; Fu, L.; Gedik, N.; Jarillo-Herrero, P. Electrically switchable Berry curvature dipole in the monolayer topological insulator WTe_2. *Nat. Phys.* **2018**, *14* (9), 900−906.

(3) Ma, Q.; Xu, S.-Y.; Shen, H.; MacNeill, D.; Fatemi, V.; Chang, T.-R.; Mier Valdivia, A. M.; Wu, S.; Du, Z.; Hsu, C.-H.; Fang, S.; Gibson, Q. D.; Watanabe, K.; Taniguchi, T.; Cava, R. J.; Kaxiras, E.; Lu, H.-Z.; Lin, H.; Fu, L.; Gedik, N.; Jarillo-Herrero, P. Observation of the nonlinear Hall effect under time-reversal-symmetric conditions. *Nature* **2019**, *565* (7739), 337−342.

(4) Kang, K.; Li, T.; Sohn, E.; Shan, J.; Mak, K. F. Nonlinear anomalous Hall effect in few-layer WTe_2. *Nat. Mater.* **2019**, *18* (4), 324−328.

(5) Isobe, H.; Xu, S.-Y.; Fu, L. High-frequency rectification via chiral Bloch electrons. *Sci. Adv.* **2020**, *6* (13), No. eaay2497.

(6) Tao, L. L.; Tsymbal, E. Y. Persistent spin texture enforced by symmetry. *Nat. Commun.* **2018**, *9* (1), 2763.

(7) Hu, L.; Huang, H.; Wang, Z.; Jiang, W.; Ni, X.; Zhou, Y.; Zielasek, V.; Lagally, M. G.; Huang, B.; Liu, F. Ubiquitous Spin-Orbit Coupling in a Screw Dislocation with High Spin Coherency. *Phys. Rev. Lett.* **2018**, *121* (6), 066401.

(8) Li, X.; Zhang, S.; Huang, H.; Hu, L.; Liu, F.; Wang, Q. Unidirectional Spin−Orbit Interaction Induced by the Line Defect in Monolayer Transition Metal Dichalcogenides for High-Performance Devices. *Nano Lett.* **2019**, *19* (9), 6005−6012.

(9) Cui, C.; Xue, F.; Hu, W.-J.; Li, L.-J. Two-dimensional materials with piezoelectric and ferroelectric functionalities. *npj 2D Mater. Appl.* **2018**, *2* (1), 18.

(10) Autere, A.; Jussila, H.; Dai, Y.; Wang, Y.; Lipsanen, H.; Sun, Z. Nonlinear Optics with 2D Layered Materials. *Adv. Mater.* **2018**, *30* (24), 1705963.

(11) Avsar, A.; Ochoa, H.; Guinea, F.; Özyilmaz, B.; van Wees, B. J.; Vera-Marun, I. J. Colloquium: Spintronics in graphene and other two-dimensional materials. *Rev. Mod. Phys.* **2020**, *92* (2), 021003.

(12) You, J.-S.; Fang, S.; Xu, S.-Y.; Kaxiras, E.; Low, T. Berry curvature dipole current in the transition metal dichalcogenides family. *Phys. Rev. B: Condens. Matter Mater. Phys.* **2018**, *98* (12), 121109.

(13) Du, Z. Z.; Wang, C. M.; Lu, H.-Z.; Xie, X. C. Band Signatures for Strong Nonlinear Hall Effect in Bilayer WTe_2. *Phys. Rev. Lett.* **2018**, *121* (26), 266601.

(14) Kim, J.; Kim, K.-W.; Shin, D.; Lee, S.-H.; Sinova, J.; Park, N.; Jin, H. Prediction of ferroelectricity-driven Berry curvature enabling charge- and spin-controllable photocurrent in tin telluride monolayers. *Nat. Commun.* **2019**, *10* (1), 3965.

(15) Absor, M. A. U.; Ishii, F. Intrinsic persistent spin helix state in two-dimensional group-IV monochalcogenide MX monolayers (M = Sn or Ge and X = S, Se, or Te). *Phys. Rev. B: Condens. Matter Mater. Phys.* **2019**, *100* (11), 115104.

(16) Sławińska, J.; Cerasoli, F. T.; Gopal, P.; Costa, M.; Curtarolo, S.; Buongiorno Nardelli, M. Ultrathin SnTe films as a route towards all-in-one spintronics devices. *2D Mater.* **2020**, *7* (2), 025026.

(17) Bian, G.; Wang, X.; Miller, T.; Chiang, T. C.; Kowalczyk, P. J.; Mahapatra, O.; Brown, S. A. First-principles and spectroscopic studies of Bi(110) films: Thickness-dependent Dirac modes and property oscillations. *Phys. Rev. B: Condens. Matter Mater. Phys.* **2014**, *90* (19), 195409.

(18) Lu, Y.; Zhou, D.; Chang, G.; Guan, S.; Chen, W.; Jiang, Y.; Jiang, J.; Wang, X.-s.; Yang, S. A.; Feng, Y. P.; Kawazoe, Y.; Lin, H. Multiple unpinned Dirac points in group-Va single-layers with phosphorene structure. *npj Comput. Mater.* **2016**, *2* (1), 16011.

(19) Pumera, M.; Sofer, Z. 2D Monoelemental Arsenene, Antimonene, and Bismuthene: Beyond Black Phosphorus. *Adv. Mater.* **2017**, *29* (21), 1605299.

(20) Jin, K.-H.; Huang, H.; Wang, Z.; Liu, F. A 2D nonsymmorphic Dirac semimetal in a chemically modified group-VA monolayer with a black phosphorene structure. *Nanoscale* **2019**, *11* (15), 7256−7262.

(21) Peng, L.; Qiao, J.; Xian, J.-J.; Pan, Y.; Ji, W.; Zhang, W.; Fu, Y.-S. Unusual Electronic States and Superconducting Proximity Effect of

Bi Films Modulated by a $NbSe_2$ Substrate. *ACS Nano* **2019**, *13* (2), 1885−1892.
(22) Dong, X.; Li, Y.; Li, J.; Peng, X.; Qiao, L.; Chen, D.; Yang, H.; Xiong, X.; Wang, Q.; Li, X.; Duan, J.; Han, J.; Xiao, W. Epitaxial Growth and Structural Properties of Bi(110) Thin Films on $TiSe_2$ Substrates. *J. Phys. Chem. C* **2019**, *123* (22), 13637−13641.
(23) Ju, S.; Wu, M.; Yang, H.; Wang, N.; Zhang, Y.; Wu, P.; Wang, P.; Zhang, B.; Mu, K.; Li, Y.; Guan, D.; Qian, D.; Lu, F.; Liu, D.; Wang, W.-H.; Chen, X.; Sun, Z. Band Structures of Ultrathin Bi(110) Films on Black Phosphorus Substrates Using Angle-Resolved Photoemission Spectroscopy. *Chin. Phys. Lett.* **2018**, *35* (7), 077102.
(24) Lu, Y.; Xu, W.; Zeng, M.; Yao, G.; Shen, L.; Yang, M.; Luo, Z.; Pan, F.; Wu, K.; Das, T.; He, P.; Jiang, J.; Martin, J.; Feng, Y. P.; Lin, H.; Wang, X.-s. Topological Properties Determined by Atomic Buckling in Self-Assembled Ultrathin Bi(110). *Nano Lett.* **2015**, *15* (1), 80−87.
(25) Kokubo, I.; Yoshiike, Y.; Nakatsuji, K.; Hirayama, H. Ultrathin Bi(110) films on Si(111)$\sqrt{3}\times\sqrt{3}$-B substrates. *Phys. Rev. B: Condens. Matter Mater. Phys.* **2015**, *91* (7), 075429.
(26) Zhang, Y.; van den Brink, J.; Felser, C.; Yan, B. H. Electrically tuneable nonlinear anomalous Hall effect in two-dimensional transition-metal dichalcogenides WTe_2 and $MoTe_2$. *2D Mater.* **2018**, *5* (4), 044001.
(27) Xiao, C.; Wang, F.; Yang, S. A.; Lu, Y.; Feng, Y.; Zhang, S. Elemental Ferroelectricity and Antiferroelectricity in Group-V Monolayer. *Adv. Funct. Mater.* **2018**, *28* (17), 1707383.
(28) Tao, L. L.; Tsymbal, E. Y. Perspectives of spin-textured ferroelectrics. *J. Phys. D: Appl. Phys.* **2021**, *54* (11), 113001.
(29) Lee, H.; Im, J.; Jin, H. Emergence of the giant out-of-plane Rashba effect and tunable nanoscale persistent spin helix in ferroelectric SnTe thin films. *Appl. Phys. Lett.* **2020**, *116* (2), 022411.
(30) Ugeda, M. M.; Bradley, A. J.; Zhang, Y.; Onishi, S.; Chen, Y.; Ruan, W.; Ojeda-Aristizabal, C.; Ryu, H.; Edmonds, M. T.; Tsai, H.-Z.; Riss, A.; Mo, S.-K.; Lee, D.; Zettl, A.; Hussain, Z.; Shen, Z.-X.; Crommie, M. F. Characterization of collective ground states in single-layer $NbSe_2$. *Nat. Phys.* **2016**, *12* (1), 92−97.
(31) Nakata, Y.; Sugawara, K.; Ichinokura, S.; Okada, Y.; Hitosugi, T.; Koretsune, T.; Ueno, K.; Hasegawa, S.; Takahashi, T.; Sato, T. Anisotropic band splitting in monolayer $NbSe_2$: implications for superconductivity and charge density wave. *npj 2D Mater. Appl.* **2018**, *2* (1), 12.
(32) Zhang, Y.; Sun, Y.; Yan, B. Berry curvature dipole in Weyl semimetal materials: An ab initio study. *Phys. Rev. B: Condens. Matter Mater. Phys.* **2018**, *97* (4), 041101.
(33) Lotsch, B. V. Vertical 2D Heterostructures. *Annu. Rev. Mater. Res.* **2015**, *45* (1), 85−109.
(34) Li, M.-Y.; Chen, C.-H.; Shi, Y.; Li, L.-J. Heterostructures based on two-dimensional layered materials and their potential applications. *Mater. Today* **2016**, *19* (6), 322−335.
(35) Zhao, A. L.; Li, H.; Hu, X. J.; Wang, C.; Zhang, H.; Lu, J. G.; Ruan, S. C.; Zeng, Y. J. Review of 2D group VA material-based heterostructures. *J. Phys. D: Appl. Phys.* **2020**, *53* (29), 293002.
(36) Wang, Z. F.; Yao, M.-Y.; Ming, W.; Miao, L.; Zhu, F.; Liu, C.; Gao, C. L.; Qian, D.; Jia, J.-F.; Liu, F. Creation of helical Dirac fermions by interfacing two gapped systems of ordinary fermions. *Nat. Commun.* **2013**, *4* (1), 1384.
(37) Yeom, H. W.; Kim, S. H.; Shin, W. J.; Jin, K.-H.; Park, J.; Kim, T.-H.; Kim, J. S.; Ishikawa, H.; Sakamoto, K.; Jhi, S.-H. Transforming a surface state of a topological insulator by a Bi capping layer. *Phys. Rev. B: Condens. Matter Mater. Phys.* **2014**, *90* (23), 235401.
(38) Jin, K.-H.; Yeom, H. W.; Jhi, S.-H. Band structure engineering of topological insulator heterojunctions. *Phys. Rev. B: Condens. Matter Mater. Phys.* **2016**, *93* (7), 075308.

https://doi.org/10.1021/acs.nanolett.1c02811
Nano Lett. 2021, 21, 9468−9475